Progress In Electromagnetics Research B, Vol. 84, 23–42, 2019

Decay Length Estimation of Single-, Two-, and Three-Wire Systems above Ground under HEMP Excitation

Salvatore Campione*, Larry K. Warne, Matthew Halligan, Olga Lavrova, and Luis San Martin

Abstract—We analytically model single-, two-, and three-wires above ground to determine the decay lengths of common and differential modes induced by an E1 high-altitude electromagnetic pulse (HEMP) excitation. Decay length information is pivotal to determine whether any two nodes in the power grid may be treated as uncoupled. We employ a frequency-domain method based on transmission line theory named ATLOG — Analytic Transmission Line Over Ground to model infinitely long and finite single wires, as well as solve the eigenvalue problem of a single-, two-, and three-wire system. Our calculations show that a single, semi-infinite power line can be approximated by a 10 km section of line and that the second electrical reflection for all line lengths longer than the decay length are below half the rated operating voltage. Furthermore, our results show that the differential mode propagates longer distances than the common mode in two- and three-wire systems, and this should be taken into account when performing damage assessment from HEMP excitation. This analysis is a significant step toward simplifying the modeling of practical continental grid lengths, yet maintaining accuracy, a result of enormous impact.

1. INTRODUCTION

The purpose of this paper is to predict the length at or above which a finite conductor interacting with a conducting ground mimics the response of a semi-infinite conductor over ground when excited by an E1 high-altitude electromagnetic pulse (HEMP). This quantity is connected to the decay length, which allows us to state that any two nodes distant more than a decay length in the grid may be treated as uncoupled. Note this definition of decay length is a multiple of the more conventional e^{-1} decay-length definition, as it will be shown later in this manuscript. Although an analysis toward this goal was reported in [1], we also consider the more relevant and general case of two and three conductors over ground, and study their eigenvalue problems to determine the decay lengths of both common and differential modes, and compare them to the single wire case. This is important as HEMP excitation can in general couple to both common and differential modes, which inherently exhibit very different propagation lengths, the latter propagating longer distances, thus potentially being an issue for damage assessment.

The analysis of a wire above a conducting ground was originally reported in [2], where a formula for the ground impedance at low frequencies was discussed. Other contributions to this problem, including approximations for the ground admittance, were reported in [3]. The exact solution of a filament above a conductive ground was provided in [4, 5]. Based on this solution, other works investigated multiple-wire modes, high-frequency modes, and buried wires [6–9]. The reader is referred to [10, 11] and references therein for a more in-depth overview of previous works on the topic, where a frequency-domain transmission line model referred to as ATLOG — Analytic Transmission Line Over Ground —

Received 8 January 2019, Accepted 9 April 2019, Scheduled 17 April 2019
* Corresponding author: Salvatore Campione (sncampi@sandia.gov).
The authors are with the Sandia National Laboratories, P. O. Box 5800, Albuquerque, NM 87185, USA.

was developed and whose results were found in good agreement with full-wave simulators. ATLOG can treat the general cases of HEMP (E1 or E2) excitation of finite or infinite lossy, insulated conductors and lossy grounds, as well as insulated conductors above, below, or resting on the ground [10, 11]. Reference works on EMP coupling to long lines along with many additional references can be found in [12–16]. In this paper, we consider overhead lines but wires close to ground (e.g., SCADA systems) and underground can also be treated. ATLOG can also treat other kinds of EMP excitation, such as source region EMP [17], as well as various terminating loading conditions [18], but these are not discussed in this manuscript. If we have an aerial line with height $h = 10\,\mathrm{m}$ and we take the radius to be small $a = 1\,\mathrm{cm}$ then the electric field at wire surface exceeds the corona threshold $E_c = 4.5\,\mathrm{MV/m}$ [19–21] for $V \geq 340\,\mathrm{kV}$ (corresponding to about $I \geq 0.8\,\mathrm{kA}$). Alternatively, if we consider a maximum voltage of $V = 3.2\,\mathrm{MV}$ the corona threshold is reached when the radius is less than $a_c = 0.15\,\mathrm{m}$. Therefore, the initial peak for maximum coupling parameters is expected to exceed the corona threshold and result in additional losses. Corona [19–21] and other nonlinear breakdown effects will not be discussed further in this paper.

The manuscript outline is as follows. In Sec. 2, we compare the time-domain results for the voltage induced on finite single lines to the result for a semi-infinite line to define the decay length. In Sec. 3, we introduce the eigenvalue problem in the frequency domain for two- and three-wire systems above ground, and compute decay lengths for both common and differential modes supported by the systems, comparing to the single wire results. Here we also make a connection between the time-domain results and the frequency-domain results via the dominant frequency of the excitation waveform. The military standard (MIL-STD) E1 HEMP waveform [22], summarized in Appendix A, is used for excitation, and the inverse transform is taken to obtain the current and the voltage on the wire as a function of time. The transmission line approximation [10, 11] under plane wave excitation is summarized in Appendix B for finite and infinite single lines and forms the basis for the approach presented in the manuscript. The required information to the eigenvalue problem is summarized in Appendix C for a single wire, as well as for common and differential modes of two- and three-wire systems.

2. DECAY LENGTH ESTIMATION USING THE ATLOG MODEL FOR SINGLE LINES

In this section, we aim to estimate the decay length of the mode supported by a single conductor above a conducting ground using the model described in Appendix B (the ground admittance will not be included in this paper because its effect is negligible for aerial lines). The single-wire line interacts with the ground through the line monopole moment. We define the decay length as the length at or above which the current and voltage on the line mimic the ones from a semi-infinite power line, and such that the second electrical reflection for all line lengths longer than the decay length is below the rated operating voltage.

Consider the schematic of a single conductor above ground as in Fig. 1(a) excited by a HEMP waveform. In general, the electric field drive exciting the line is given as a combination of transverse electric (TE) and transverse magnetic (TM) field components as

$$\mathrm{Drive} = \mathbf{E}_{\mathrm{tot}} \cdot \mathbf{e}_z = -E_{\mathrm{tot}}^{\mathrm{TE}} \sin\Phi + E_{\mathrm{tot}}^{\mathrm{TM}} \cos\Phi \sin\Psi \tag{1}$$

where $\mathbf{E}_{\mathrm{tot}}$ is the total electric field drive along the line; $\mathbf{e}_z$ is the unit vector along the direction of the line; $E_{\mathrm{tot}}^{\mathrm{TE,\,TM}}$ are the total TE and TM components of the exciting field; Φ indicates the orientation of the line versus the driving field; and Ψ is the incidence angle. The time harmonic convention $\exp(-i\omega t)$ is implicitly assumed in this paper.

It has been shown in [10, 15] that the largest coupling to the line is generally achieved near grazing incidence for $\Phi = 0$ when the line is excited by a TM incident plane wave polarized in the plane containing the wire and the ground surface with incidence angle Ψ with respect to the z axis as shown in Fig. 1(b). Therefore, we will concentrate on this latter case in this paper, assuming a MIL-STD waveform dependence as in Appendix A, but a general excitation can be easily solved for.

From Fig. 1(b), we note that the parameters that enter our simulations are ground permittivity ε_4, ground conductivity σ_4, wire radius a, coating radius b, wire conductivity σ_0, height h, and wire length L. In this paper, unless otherwise specified, we assume $\varepsilon_4 = 20\varepsilon_0$, $\sigma_4 = \{0.001, 0.01, 0.1\}\,\mathrm{S/m}$,

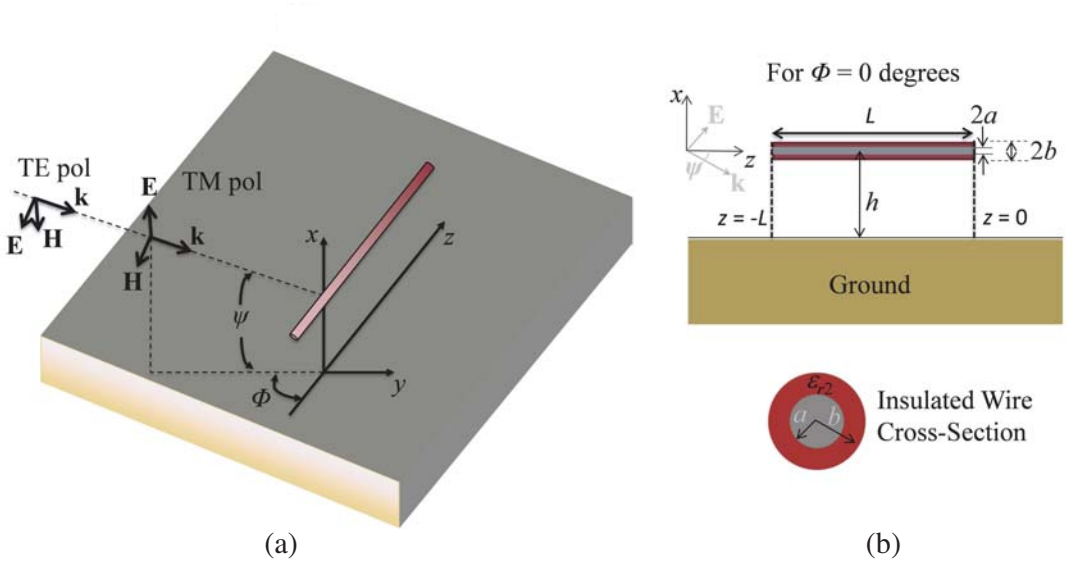

(a) (b)

Figure 1. (a) Schematic of a single conductor above ground excited by a HEMP waveform. (b) Simplification of panel (a) for a conductor with length L under TM excitation only for $\Phi = 0$, generally inducing the largest coupling to the line near grazing incidence. The semi-infinite case is obtained assuming $L = \infty$.

$a = 1\,\text{cm}$ (no coating), $\sigma_0 = 2.9281 \times 10^7\,\text{S/m}$, $h = 10\,\text{m}$, and various $L = \{1, 2, 5, 10, 50\}\,\text{km}$. We note that the ground conductivity value of $\sigma_4 = 0.01\,\text{S/m}$ is typical, and we analyze also the extreme cases of $\sigma_4 = 0.001\,\text{S/m}$ and $\sigma_4 = 0.1\,\text{S/m}$ to have a complete survey of its effect on the decay length.

Using the model in Appendix B, in Fig. 2(a) we consider five finite lines of lengths 1 km, 2 km, 5 km, 10 km, and 50 km at the height of 10 m, and compute the voltage at the right termination of the line under the MIL-STD HEMP waveform in Appendix A incident at an angle $\Psi = \pi/33$, assuming the terminations to be loaded with $Z_L^{\pm} = 1\,\text{G}\Omega$ (resembling an open circuit). Although other loading conditions are not analyzed here, this analysis allows us to determine the decay length; other more realistic loading conditions to take into account connections to transformers, lightning arrestors, etc. will be considered in future work. This near-grazing angle $\Psi = \pi/33$ has been identified as the angle leading to the largest coupling to the line for $\sigma_4 = 0.01\,\text{S/m}$; other angles would induce lower voltages and currents, see for example [10, 15]. Note the delay due to the propagation through the line, $\Delta t = L/c$ where c is the speed of light, has been subtracted from the time span in Fig. 2 to enable comparisons among the various results. We compare these results to the one of a semi-infinite long line. We observe that, concerning the peak voltage of the right termination, any line length above 5 km leads to the same peak voltage result of about 3.2 MV. This result confirms that any line longer than 5 km in the grid may be treated as an uncoupled line.

The peak voltage, full-width at half maximum (FWHM), and the difference (with respect to the semi-infinite line) in Energy $= \int_0^T Z_L^+ I^2 dt$ (with $T = 1000\,\text{ns}$, imposed to take into account only the main peak, and not late-time reflections) in Fig. 2(a) from the finite line results are reported in Table 1 (note that much larger energies would be achieved with a load matched to the characteristic impedance of the line). For lines longer than 5 km, most of the energy is already contained in the pulse versus the semi-infinite case. Fig. 2(a) and Table 1 illustrate that the decay length of a semi-infinite single-conductor of coupling is approximately between 10 and 50 km (e.g., in numerical computations, this means that a semi-infinite line can be approximated with a 10 km line (resulting in less than 6% error in energy), or 50 km line (resulting in less than 3% error in energy)). This is an important result, which means that, for large electrical power systems, any two buses or locations greater than 10 to 50 km apart can be simulated as decoupled buses or nodes for E1 HEMP coupling computations. Such relaxation in computational intensity will, for the first time, allow us to carry out direct numerical analysis of

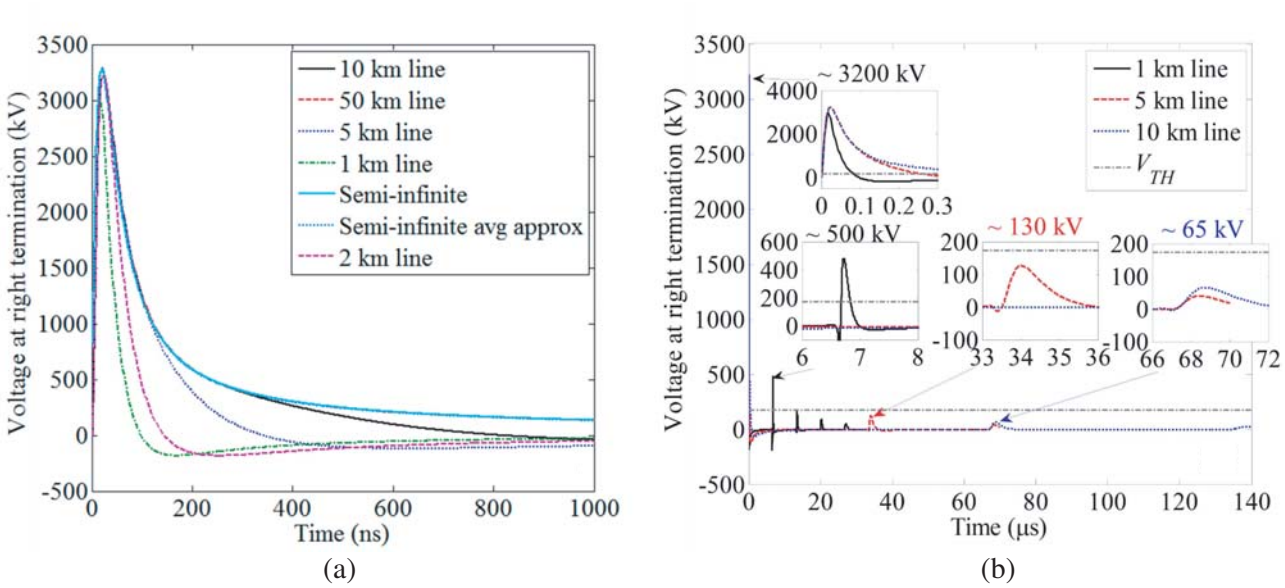

Figure 2. (a) Voltage versus time at the angle of incidence of $\Psi = \pi/33$ using ATLOG for various finitely long wires above ground under a MIL-STD HEMP waveform with $\sigma_4 = 0.01\,\mathrm{S/m}$. The voltage is computed at the right termination of the wire, and the delay $\Delta t = L/c$ in the finite lines has been subtracted to enable comparisons among the various results. (b) As in (a), but for longer times to see the reflections from the other end of the line.

Table 1. Peak voltage, full-width at half maximum (FWHM), energy, and energy relative difference Δ to the semi-infinite line result of the pulses in Fig. 2(a).

Line length (km)	V_{peak} (MV)	FWHM (ns)	Energy (mJ)	Δ (%)
Semi-infinite	3.2	71.12	0.654	0.00
50	3.2	71.12	0.636	2.75
10	3.2	71.12	0.618	5.50
5	3.2	71.12	0.575	12.08
2	3.2	50.91	0.413	36.85
1	2.99	32.92	0.226	65.44

medium- to large-scale power systems.

To further validate the fact that buses (nodes) far apart can be treated as decoupled, as well as to understand if any reflections need to be considered in HEMP waveform coupling and propagating within the electrical grid, we have conducted a longer (in time) simulation shown in Fig. 2(b) for finite lines of lengths 1 km, 5 km, and 10 km. In general, if L is the length of the line, a reflection peak may appear at a time $t_{R,n} = 2Ln/c$, where c is the speed of light and n indicates the nth reflection. For the 1 km line, we observe multiple reflection peaks, with the first one appearing at $t_{R,1} = 6.67\,\mu\mathrm{s}$ with a voltage level of about 500 kV (see inset in Fig. 2(b)). Considering a 345 kV power line and assuming that transformers may withstand voltage levels up to $1.5V_{AC}$, taking this reflection to appear at a peak time of the 60 Hz signal, imposes a threshold $V_{TH} = 0.5V_{AC} = 172.5\,\mathrm{kV}$. Therefore, we would need to take into consideration the first reflection of the 1 km line for damage considerations. For longer lines, however, the first reflection voltage peak in Fig. 2(b) is below V_{TH}, being 130 kV for the 5 km line and 65 kV for the 10 km line (see insets in Fig. 3(b)), again confirming that lines larger than 5 km in the grid may be treated as uncoupled lines. We summarize this information in Table 2 for various voltage ratings of lines found in the power grid.

Note that this prior length is a multiple of the more conventional e^{-1} decay-length definition,

Table 2. Minimum line lengths to ignore the first reflection for damage considerations for typical voltage ratings of power lines.

Voltage rating (kV)	135	345	1000
Minimum line length (km)	10	5	1

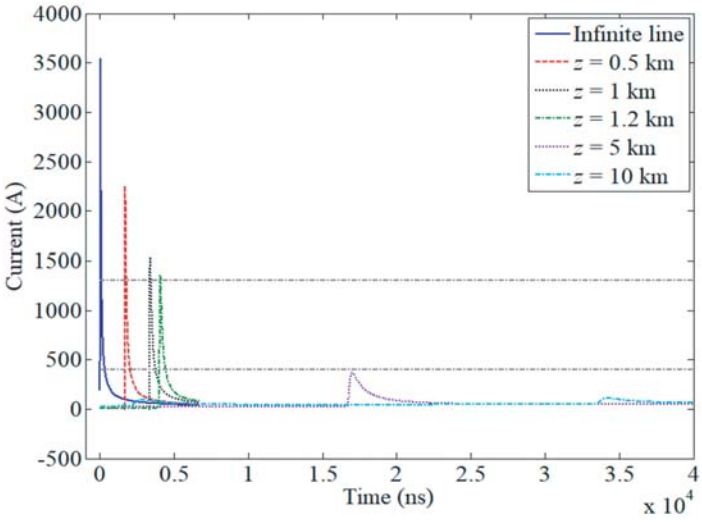

Figure 3. Current versus time at different locations z along the wire from Eq. (2), assuming a semi-infinite line driven by a Norton equivalent circuit.

which is about 1200 m. To estimate both of these lengths in a clearly defined setting, we retrieve the current induced on an infinite line at $z = 0$, given by $I_i = -YA_0/(\Gamma^2 - k_0^2 \cos^2\theta_0)e^{ik_0 z\cos\theta_0}$, and use a matched Norton equivalent circuit to feed a semi-infinite line for which the solution satisfying the radiation condition as $z \to +\infty$ is

$$I = A_1 e^{i\Gamma z}, \quad V = -i\Gamma \frac{A_1}{Y} e^{i\Gamma z}, \tag{2}$$

with $A_1 = 2I_i/(1 - i\Gamma Y_0/Y)$ and $Y_0 = \sqrt{Y/Z}$. This is done to use the actual time dependence of the expected waveform, avoiding complications due to reflections from line terminations as observed in Fig. 2(b). We plot in Fig. 3 the current versus time at different z-locations along the wire from Eq. (2). One can see that the value $e^{-1}I_{\text{peak}}$ is achieved after about 1200 m. Furthermore, one can define a current threshold as $I_{TH} = V_{TH}/\zeta_{\text{peak}}$ (with the approximate characteristic impedance of the line $\zeta_{\text{peak}} \approx 430\,\Omega$ at a frequency representing the pulse width), and again the current is below this value after 5 km, in agreement with the result in Fig. 2(b).

We now consider in Fig. 4 the same case of Fig. 2(b), but with larger ($\sigma_4 = 0.1$ S/m) and smaller ($\sigma_4 = 0.001$ S/m) ground conductivity. We observe that for larger ground conductivity, slightly longer lines are needed not to worry about the reflections from the other termination, whereas for smaller ground conductivity the threshold requirement is already satisfied. Therefore, for $\sigma_4 < 0.01$ S/m, lines larger than 5 km in the grid may be treated as uncoupled lines, while lines larger than 10 km are required for $\sigma_4 = 0.1$ S/m.

3. ANALYSIS OF A TWO-WIRE SYSTEM ABOVE GROUND

We now consider the more complex scenario of a two-wire system above ground, where two modes, common and differential, may be induced by a HEMP excitation. The two-wire system differential mode interacts with the ground through the line dipole moment. These modes may decay with different length scales, and it is our aim to determine their decay lengths. This is important because a HEMP

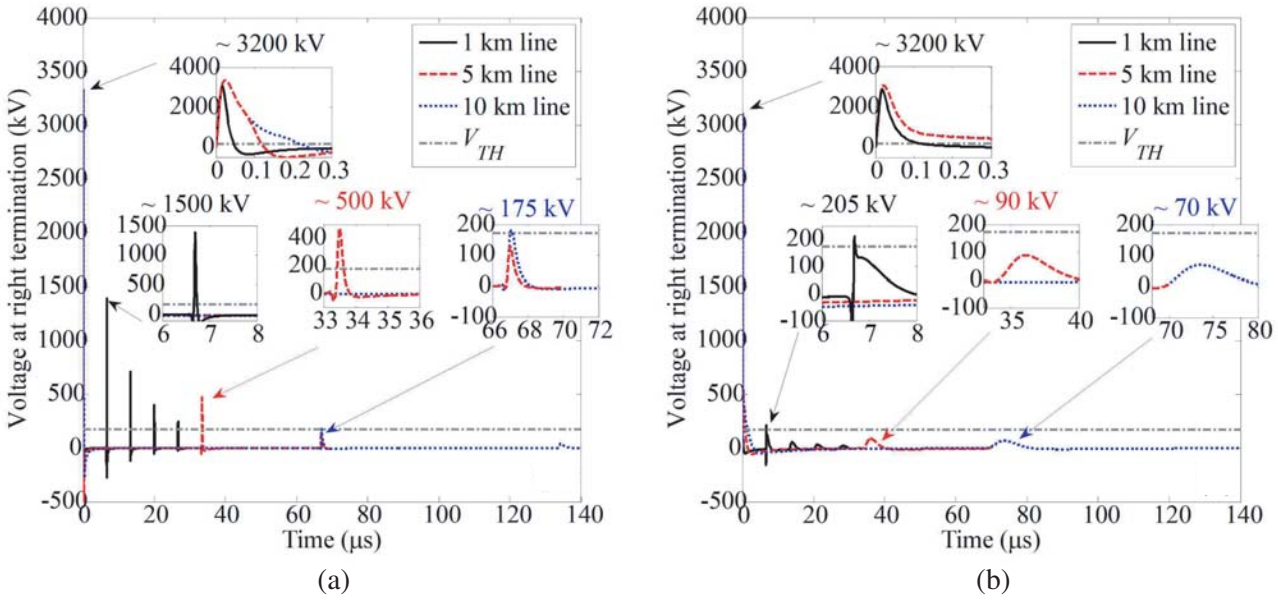

Figure 4. (a) As in Fig. 2(b), but with $\sigma_4 = 0.1\,\mathrm{S/m}$. (b) As in Fig. 2(b), but with $\sigma_4 = 0.001\,\mathrm{S/m}$.

excitation can in general couple to either mode, and full knowledge is required to comment on damage assessment.

3.1. Eigenvalue Problem for a Two-Wire System

Figure 5 shows the schematic of two horizontally displaced (along x, with displacement 2Δ) wires at a height h above a conducting ground. The two wires are along the z direction. We are interested in assessing the conventional e^{-1} decay-length of common and differential modes supported by the two-wire system, through which we can define whether any two nodes in the grid are distant enough to be treated as uncoupled. Note this arrangement of wires is typical of power lines and SCADA components; other arrangements will be investigated in the future.

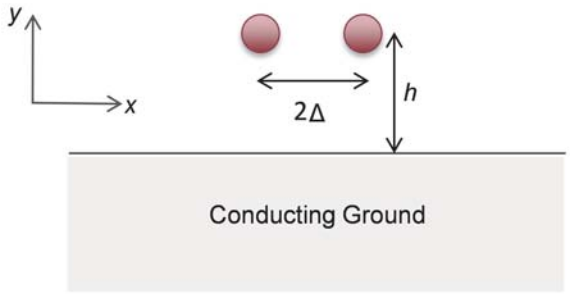

Figure 5. Schematic cross section of two identical wires above a conducting ground that are displaced along x at a height h. Note the wires are along the z direction.

The vector transmission line equations of the two-wire system for current and voltage are

$$\frac{d}{dz}\underline{V} = -\underline{Z}\cdot\underline{I}; \quad \frac{d}{dz}\underline{I} = -\underline{Y}\cdot\underline{V} \tag{3}$$

where the admittance matrix $\underline{Y}$, the impedance matrix $\underline{Z}$, the voltage vector $\underline{V}$, and the current vector

$\underline{I}$ are given by

$$\underline{Z} = \begin{pmatrix} Z_{++} & Z_{+-} \\ Z_{-+} & Z_{--} \end{pmatrix}; \quad \underline{Y} = \begin{pmatrix} Y_{++} & Y_{+-} \\ Y_{-+} & Y_{--} \end{pmatrix}; \quad \underline{V} = \begin{pmatrix} V_+ \\ V_- \end{pmatrix}; \quad \underline{I} = \begin{pmatrix} I_+ \\ I_- \end{pmatrix} \tag{4}$$

If we eliminate the voltage from Eq. (3) we obtain

$$\frac{d^2}{dz^2}\underline{I} = \underline{Y} \cdot \underline{Z} \cdot \underline{I} = \lambda \underline{I} \tag{5}$$

with solutions $\underline{I} = \underline{c}e^{\pm z\sqrt{\lambda}}$, amplitudes $\underline{c}$, and propagation constant $\sqrt{\lambda}$, whose eigenvectors satisfy $\underline{Y} \cdot \underline{Z} \cdot \underline{I} = \lambda \underline{I}$ and with λ an eigenvalue of the system, computed using $|\underline{Y} \cdot \underline{Z} - \lambda| = 0$. Guidelines to find the decay length of a single wire as well as the two-wire system are reported in Appendix C.2.

We assume that the two wires are symmetrical, e.g., $a_+ = a_- = a$, with the same height $h_+ = h_- = h$ and placed at $x_\pm = \pm\Delta$ as in Fig. 5. All the other parameters are as in Sec. 3, with $\sigma_4 = 0.01\,\mathrm{S/m}$. In this case, we note that $Y_{++} = Y_{--} = Y$ and $Z_{++} = Z_{--} = Z$ (expressions for all these terms can be found in Appendix C). We note that $Y_{+-} = Y_{-+} = Y_m$ and $Z_{+-} = Z_{-+} = Z_m$, so that

$$\underline{Y} \cdot \underline{Z} = \begin{pmatrix} YZ + Y_m Z_m & YZ_m + Y_m Z \\ Y_m Z + YZ_m & Y_m Z_m + YZ \end{pmatrix} \tag{6}$$

Following Appendix C.2 and solving for the eigenvalues through $|\underline{Y} \cdot \underline{Z} - \lambda| = 0$, we obtain $\lambda_1 = (Y - Y_m)(Z - Z_m)$ and $\lambda_2 = (Y + Y_m)(Z + Z_m)$. The first eigenvector satisfies $\begin{pmatrix} 1 & 1 \\ 1 & 1 \end{pmatrix}\underline{I}_1 = 0$, with $\underline{I}_1 = \begin{pmatrix} 1 \\ -1 \end{pmatrix}$, representing a differential mode current, while the second eigenvector satisfies $\begin{pmatrix} -1 & 1 \\ 1 & -1 \end{pmatrix}\underline{I}_2 = 0$, with $\underline{I}_2 = \begin{pmatrix} 1 \\ 1 \end{pmatrix}$, representing a common mode current. These two eigenvectors propagate along the line without cross-coupling. The inverse decay length of the differential mode is $\mathrm{Re}\sqrt{\lambda_1} = \mathrm{Re}\sqrt{(Y - Y_m)(Z - Z_m)}$ and the inverse decay length of the common mode is $\mathrm{Re}\sqrt{\lambda_2} = \mathrm{Re}\sqrt{(Y + Y_m)(Z + Z_m)}$.

The inverse decay lengths of common mode with and without wire loss are shown in Fig. 6 versus frequency for various values of separation 2Δ, neglecting the effects of the ground admittance. Looking

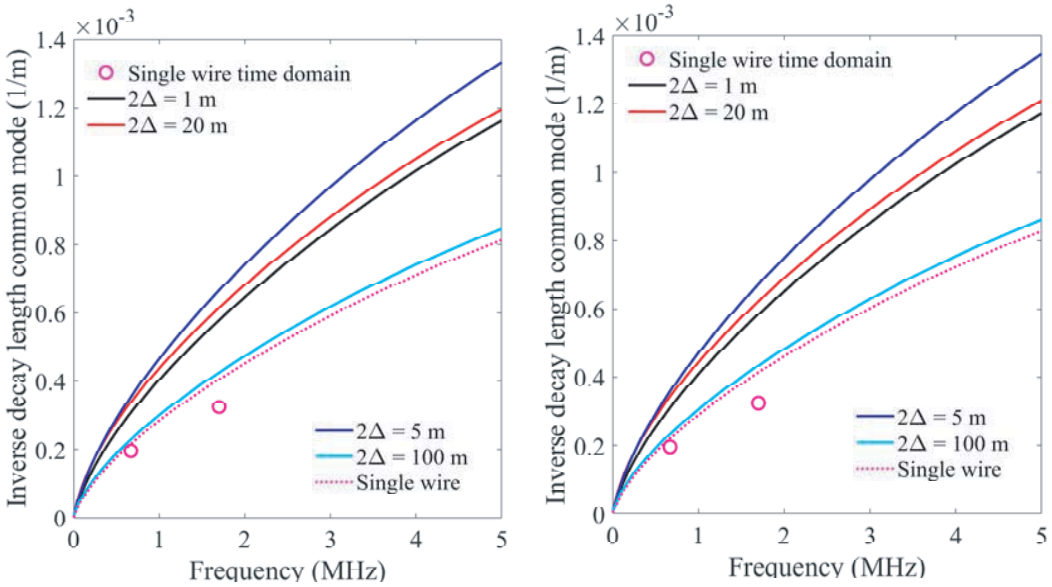

Figure 6. Inverse decay lengths for various values of separation 2Δ for the common mode (a) without and (b) with wire losses for two wires above ground with $h = 10\,\mathrm{m}$.

at the results for the common mode in Fig. 6, we observe that wire loss has a negligible effect on its decay length. We see that for increasing separation, the loss increases, peaking at about $2\Delta = 5\,\text{m}$. Further increasing the wire separation reduces the loss, and the result resembles again the single wire result for very large separation $2\Delta \geq 100\,\text{m}$ (see Appendix C.1 for more information about the decay length of a single wire). This can be explained as follows. Because the equivalent radius of an isolated wire pair $a_e = \sqrt{2\Delta a}$ increases as the two wires move apart, we see that the free space inductance per unit length $L_e = \mu_0 \ln(2h/a_e)/2\pi$ decreases, but the part of the impedance per unit length from the ground Z^{fi} remains essentially fixed. Hence, for increasing wire radii we reduce the external part of the impedance per unit length and thus increase the influence of the ground part of the impedance per unit length, with a resulting increase in decay constant from the losses in the ground. This effect is analogous to breaking up a single wire into two wires as in the common mode of the two wires here analyzed, when the wires are still close together compared to the distance to the ground. As the wires become widely separated compared to the wire height to the ground, we then have the parallel combination

$$\begin{aligned} C_e^{tot} &\to 2C_e \\ Z^{tot} &\to Z/2 = \left(-i\omega L_e + Z^{fi}\right)/2 \end{aligned} \tag{7}$$

and the propagation constant for the parallel combination becomes $\Gamma^{tot} = \sqrt{-Z^{tot}Y^{tot}} \to \sqrt{i\omega C_e Z}$, the same result as for a single wire in Appendix C.1. Hence, these simple results explain why we initially see an increase in decay constant, followed by a return to the single wire decay at wide separation distances. An equivalent radius model for the common mode of a two-wire system is given in Appendix C.3.

In Fig. 6, we also report the single wire inverse decay length for comparison as well as the result coming from the time domain data in Fig. 2(b). The latter is computed as follows: looking at the 5 km and 10 km lines (red and blue curves in Fig. 2(b), respectively), one can determine the dominant frequency as $f = 1/(2T_p)$, where T_p is the pulse duration, equal to about 300 ns for the 5 km line and about 740 ns for the 10 km line. Looking at the voltage levels at initial peak P_0 and first reflection peak P_1, we can compute a decay length as $d = (2L)/\ln(P_0/P_1)$. For example, for the 5 km line, $d = (2 \cdot 5000)/\ln(3219/125.8) \sim 3084\,\text{m}$, whose order of magnitude is of the same order of what found

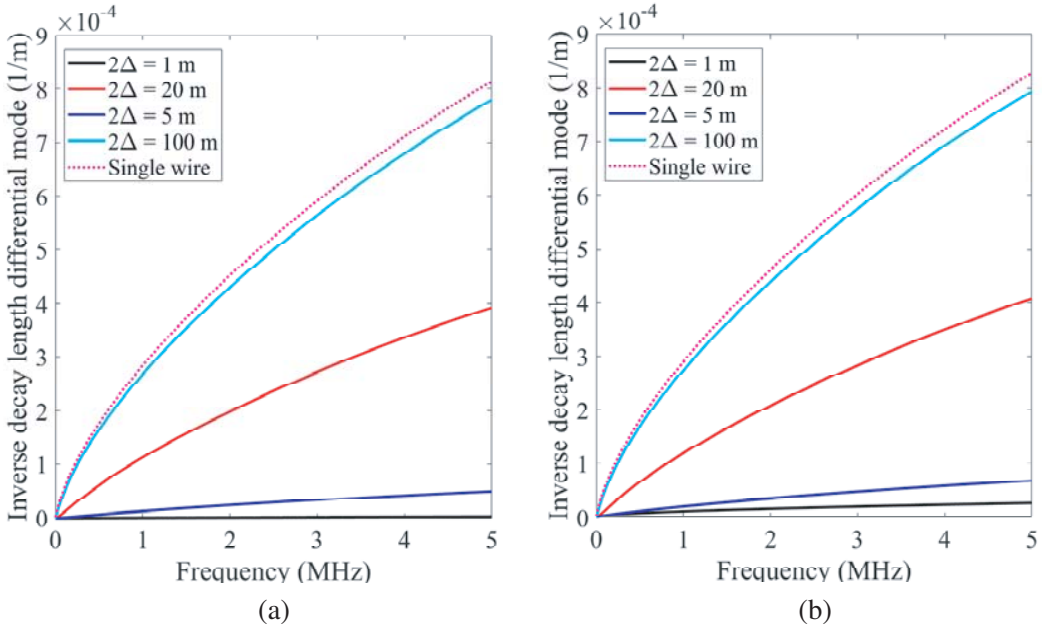

Figure 7. Inverse decay lengths for various values of separation 2Δ for the differential mode (a) without and (b) with wire losses for two wires above ground with $h = 10\,\text{m}$. In panel (a), the case with $2\Delta = 1\,\text{m}$ (black curve) has an inverse decay length of $2.8 \times 10^{-6}\,1/\text{m}$ at 5 MHz and exhibits a similar shape as the other cases here illustrated.

in Fig. 3. The fact that the symbols in Fig. 6 follow the single wire result (magenta curve) shows that we can estimate the decay from the dominant frequency $f = 1/(2T_p)$. This is an important result as the decay length at the dominant frequency can be easily and quickly calculated.

We now look at the differential mode results in Fig. 7. One can see that, compared to the common mode, the differential mode travels longer distances for the same decay amount, especially for close wires for which $2\Delta \ll h$. For example, when $2\Delta = 5\,\text{m}$ and at 1 MHz, the common mode has a decay length of about 2.1 km, while the differential mode has a decay length of about 49.1 km. We see that the wire loss has a great effect, especially for close wires, e.g., $2\Delta = 1\,\text{m}$; for $2\Delta = 5\,\text{m}$, the effect is present but not large. For very large separation $2\Delta \geq 100\,\text{m}$, the differential mode result resembles the single wire result.

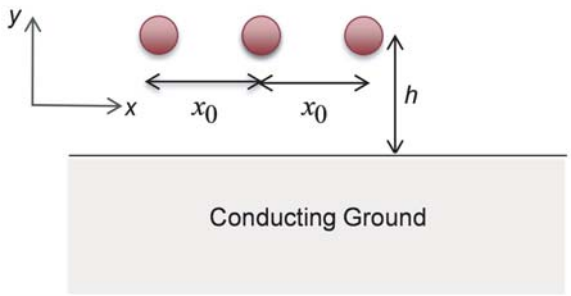

Figure 8. Schematic cross section of three identical wires above a conducting ground that are displaced along x at a height h. Note the wires are along the z direction.

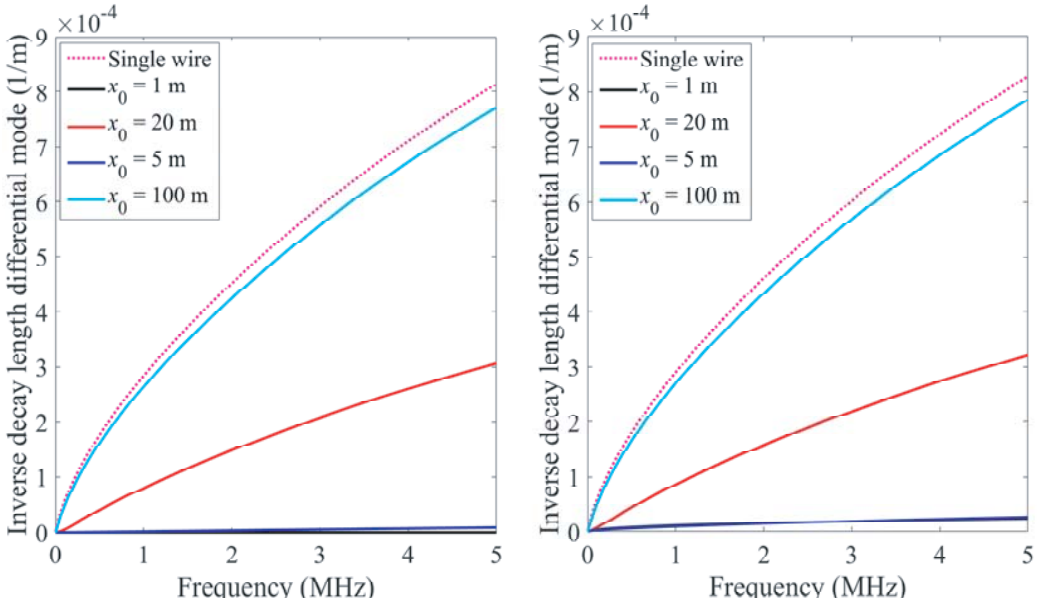

Figure 9. Inverse decay lengths for various values of separation x_0 for the differential mode (a) without and (b) with wire losses for two wires above ground with $h = 10\,\text{m}$. In panel (a), the case with $x_0 = 1\,\text{m}$ (black curve) has an inverse decay length of $2.4 \times 10^{-8}\,1/\text{m}$ at 5 MHz and exhibits a similar shape as the other cases here illustrated. In panel (b), the case with $x_0 = 1\,\text{m}$ (black curve) is very similar to the case with $x_0 = 5\,\text{m}$ (blue curve).

4. ANALYSIS OF A THREE-WIRE SYSTEM ABOVE GROUND: INTERACTION THROUGH THE LINE QUADRUPOLE MOMENT

We now consider a three-wire system above ground (a more realistic configuration), where three modes may be induced by a HEMP excitation. A particular differential mode on the three-wire line can be selected to interact with the ground only through the line quadrupole moment (see Appendix C.4). This opens the possibility of a smaller loss (and thus longer decay lengths) for this particular three-wire line mode.

Figure 8 shows the schematic of three horizontally displaced (along x, with displacement x_0) wires at a height h above a conducting ground. The three wires are along the z direction.

The inverse decay lengths of the three wire differential (quadrupolar) mode with and without wire loss are shown in Fig. 9 versus frequency for various values of separation x_0. One can see that, compared to the differential mode of two wires, this mode travels longer distances for the same decay amount, especially for close wires for which $x_0 \ll h$. We see that the wire loss has a great effect, especially for close wires, e.g., $x_0 = 1\,\mathrm{m}$, and even for $x_0 = 5\,\mathrm{m}$. For very large separation $x_0 \geq 100\,\mathrm{m}$, also this differential mode result resembles the single wire result.

5. CONCLUSION

In this paper, we analytically model single-wire, two-wire, and three-wire systems for typical overhead conductor infrastructure to determine the decay length of current and voltages induced by an E1 HEMP excitation. Because in general this can couple to both common and differential modes, their decay properties need to be taken into account for damage assessment. In particular, for a single wire, we have shown that the first reflection for all line lengths analyzed *greater* than the decay length are below the threshold of half nominal rated operating voltage. This is a very important result, confirming that electrical buses further than a decay length apart can be considered decoupled, and that a first (and later) reflections do not contribute to over-voltages greater than half the nominal. Thus, we should not expect reflections from further than a decay length to contribute to failures or damages to equipment. Through a numerical computation we have established a threshold (in time and space) for potential failures and damages of electric utility assets following a HEMP event. Our results show that the differential modes in two- and three-wire systems propagate longer distances than the common mode, and that wire losses dramatically affect their decay length, especially for close wires. We have computed the decay length using two distinct approaches, one in the time domain, and one solving the eigenvalue problem in the frequency domain. The two have shown similar conclusions, strengthening our understanding of the modeling of these kinds of coupling problems.

ACKNOWLEDGMENT

This work was supported by the Laboratory Directed Research and Development program at Sandia National Laboratories. Sandia National Laboratories is a multimission laboratory managed and operated by National Technology and Engineering Solutions of Sandia, LLC, a wholly owned subsidiary of Honeywell International, Inc., for the U.S. Department of Energy's National Nuclear Security Administration under contract DE-NA-0003525. This paper describes objective technical results and analysis. Any subjective views or opinions that might be expressed in the paper do not necessarily represent the views of the U.S. Department of Energy or the United States Government.

APPENDIX A. ELECTROMAGNETIC PULSE WAVEFORM AND SPECTRUM USED IN THIS PAPER

We describe here the MIL-STD E1 HEMP electromagnetic pulse waveform we employ in this paper. A double exponential characterization of the waveform is [22, 23]

$$E(t) = KE_0\left(e^{-\alpha t} - e^{-\beta t}\right)u(t), \tag{A1}$$

with $E_0 = 50\,\mathrm{kV/m}$, $\alpha = 4 \times 10^7\,\mathrm{s}^{-1}$, $\beta = 6 \times 10^8\,\mathrm{s}^{-1}$, and $K = 1/(e^{-\alpha t_{\max}} - e^{-\beta t_{\max}})$ a normalization constant, with $t_{\max} = \log(\beta/\alpha)/(\beta - \alpha)$, $u(t) = 0$ for $t < 0$, and $u(t) = 1$ for $t \geq 0$. Its spectrum is given by (assuming an $\exp(-i\omega t)$ time dependence)

$$E(\omega) = \int_{-\infty}^{\infty} E(t)\, e^{i\omega t} dt = \frac{E_0 K(\beta - \alpha)}{(\alpha - i\omega)(\beta - i\omega)}. \tag{A2}$$

APPENDIX B. ATLOG MODEL FOR SEMI-INFINITE AND FINITE LINES

B.1 ATLOG Model for Infinite and Semi-infinite Lines

For the uniform height transmission line running for $-\infty < z \leq z_0 = 0$ (assuming an $\exp(-i\omega t)$ time dependence), we can write differential equations for the voltage V and the current I as

$$\begin{aligned} \frac{dV}{dz} &= E_z^{inc} - ZI, \\ \frac{dI}{dz} &= -YV. \end{aligned} \tag{B1}$$

Eliminating the voltage leads to

$$\frac{d^2 I}{dz^2} + \Gamma^2 I = -Y E_z^{inc}, \tag{B2}$$

with $E_z^{inc} = A_0 e^{ik_0 z \cos\Psi}$, $\Gamma^2 = -ZY$, Ψ is the incidence angle, $k_0 = \omega/c = \omega\sqrt{\varepsilon_0 \mu_0}$ the free space wavenumber, ω the angular frequency, c the speed of light, ε_0 the free space dielectric absolute permittivity, μ_0 the free space magnetic absolute permeability, $A_0 = E_s(\omega)\sin\Psi e^{-ihk_0 \sin\Psi}(1 - R_H e^{2ihk_0 \sin\Psi})$, and $R_H = \frac{(k_4/k_0)^2 \sin\Psi - \sqrt{(k_4/k_0)^2 - \cos^2\Psi}}{(k_4/k_0)^2 \sin\Psi + \sqrt{(k_4/k_0)^2 - \cos^2\Psi}}$. For overhead power lines, i.e. $h > b$, it is frequently convenient to set the phase reference on the wire itself at $x = 0$ which can be done by setting $E_s(\omega) = E(\omega) e^{ihk_0 \sin\Psi}$, where $E(\omega)$ represents the spectrum of the incident electromagnetic pulse Appendix A. Moreover, $Z = Z_0 + Z_2 + Z_4$, where Z_2 takes into account the presence of any coating layer, Z_4 takes into account the losses in the ground, and Z_0 takes into account the losses in the wire. The admittance is given by $\frac{1}{Y} = \frac{1}{Y_e} + \frac{1}{Y_4}$, where Y_e is the external admittance and Y_4 is the ground admittance (which we neglect in this paper for aerial lines). Expressions for all these impedance and admittance terms can be found in [10, 11]. In these formulas, $k_4^2 = \omega\mu_0(\omega\varepsilon_4 + i\sigma_4)$, ε_4 is the ground permittivity, σ_4 is the ground conductivity, and h is the distance of the transmission line from the conducting ground plane.

The solution satisfying the radiation condition as $z \to -\infty$ is then

$$\begin{aligned} I &= -\frac{YA_0}{\Gamma^2 - k_0^2 \cos^2\Psi} e^{ik_0 z \cos\Psi} + A_1 e^{-i\Gamma z}, \\ V &= \frac{iA_0 k_0 \cos\Psi}{\Gamma^2 - k_0^2 \cos^2\Psi} e^{ik_0 z \cos\Psi} + i\Gamma \frac{A_1}{Y} e^{-i\Gamma z}. \end{aligned} \tag{B3}$$

For an open circuit condition at $z = z_0 = 0$, we get $\frac{A_1}{Y} = \frac{A_0}{\Gamma^2 - k_0^2 \cos^2\Psi}$, and the open circuit voltage is

$$V_{oc}(z_0) = \frac{iA_0}{\Gamma - k_0 \cos\Psi}. \tag{B4}$$

Turning the sources off, the impedance looking to the left of a semi-infinite line is $Z(z_0) = Z_0$. Note that the voltages discussed here are scattered voltages as we have not added the voltage from the transverse incident field for an open circuit. For the uniform height transmission line running for $-\infty < z < \infty$, the current is obtained using Eq. (B3) with $A_1 = 0$.

B.2 ATLOG Model for Finite Lines

If the line is of finite length $z_- \leq z \leq z_+$, rather than semi-infinite as assumed in Appendix B.1, the current and voltage are given by

$$\begin{aligned} I(z) &= [K_1 + P(z)]\, e^{-\gamma_L z} + [K_2 + Q(z)]\, e^{\gamma_L z}, \\ V(z) &= \sqrt{\frac{Z}{Y}} \left\{ [K_1 + P(z)]\, e^{-\gamma_L z} - [K_2 + Q(z)]\, e^{\gamma_L z} \right\}, \end{aligned} \tag{B5}$$

with $P(z) = \frac{1}{2}\sqrt{Y/Z} \int_{z_-}^{z} e^{\gamma_L z} E_z^{\text{inc}}(z) dz$, $Q(z) = \frac{1}{2}\sqrt{Y/Z} \int_{z}^{z_+} e^{-\gamma_L z} E_z^{\text{inc}}(z) dz$, $\gamma_L^2 = ZY$, and

$$\begin{aligned} K_1 &= \rho_- e^{\gamma_L z_-} \frac{\rho_+ P(z_+)\, e^{-\gamma_L z_+} - Q(z_-)\, e^{\gamma_L z_+}}{e^{\gamma_L (z_+ - z_-)} - \rho_- \rho_+ e^{-\gamma_L (z_+ - z_-)}}, \\ K_2 &= \rho_+ e^{-\gamma_L z_+} \frac{\rho_- Q(z_-)\, e^{\gamma_L z_-} - P(z_+)\, e^{-\gamma_L z_-}}{e^{\gamma_L (z_+ - z_-)} - \rho_- \rho_+ e^{-\gamma_L (z_+ - z_-)}}, \end{aligned} \tag{B6}$$

where the reflection coefficients at positions z_- and z_+ are $\rho_- = (Z_L^- - \sqrt{Z/Y})/(Z_L^- + \sqrt{Z/Y})$ and $\rho_+ = (Z_L^+ - \sqrt{Z/Y})/(Z_L^+ + \sqrt{Z/Y})$, determined from the terminating impedances Z_L^- and Z_L^+ to the transmission line (at locations z_- and z_+, respectively). Note that Eq. (B6) is valid for very high impedance loads, and this can be generalized by adding end generators as in [10].

This model is powerful when the drive field is varying in some complicated way with z. In this case, we can treat the finite line as in Eq. (B3) with a second reflection term for which

$$I = -\frac{YA_0}{\Gamma^2 - k_0^2 \cos^2\theta_0} e^{ik_0 z \cos\theta_0} + A_1 e^{-i\Gamma z} + A_2 e^{i\Gamma z}, \tag{B7}$$

which, for an open circuit condition at both ends at $z_- = 0$ and $z_+ = L$, we get

$$\begin{aligned} A_1 &= \frac{YA_0}{\Gamma^2 - k_0^2 \cos^2\theta_0} \frac{e^{i\Gamma L} - e^{ik_0 L \cos\theta_0}}{e^{i\Gamma L} - e^{-i\Gamma L}}, \\ A_2 &= \frac{YA_0}{\Gamma^2 - k_0^2 \cos^2\theta_0} \frac{e^{ik_0 L \cos\theta_0} - e^{-i\Gamma L}}{e^{i\Gamma L} - e^{-i\Gamma L}}. \end{aligned} \tag{B8}$$

APPENDIX C. SINGLE-WIRE, TWO-WIRE, AND THREE-WIRE MODEL

C.1. Single Wire Modal Solution Based on Carson

Maxwell's equations can be rewritten in terms of a scalar potential ϕ and a vector potential A as

$$\left(\nabla^2 + k_0^2\right) A = -\mu_0 J; \quad \left(\nabla^2 + k_0^2\right) \phi = -\rho/\varepsilon_0 \tag{C1}$$

with J the electric current density and ρ the volume charge density.

For low frequencies we drop the k_0^2 term in Eq. (C1), leading to $\nabla^2 A_z \approx -\mu_0 J_z$. Taking a negative z-directed current filament $J_z = -I\delta(x)\delta(y-h)$, we have $\nabla^2 A_z = \mu_0 I \delta(x)\delta(y-h)$. Using the two-dimensional Green's function $\nabla^2 G = \delta(\rho - \rho')$, with $G = -\ln|\rho - \rho'|/(2\pi)$ for a perfectly conducting ground interface the filament and its image give

$$A_z^p = \frac{\mu_0 I}{2\pi} \ln\left[\frac{\sqrt{x^2 + (y-h)^2}}{\sqrt{x^2 + (y+h)^2}}\right] = -\frac{\mu_0 I}{2\pi} \int_0^\infty \left[e^{-\alpha|y-h|} - e^{-\alpha|y+h|}\right] \cos(\alpha x) \frac{d\alpha}{\alpha} \tag{C2}$$

Thus, the total potential above the ground interface can be written as

$$A_z = A_z^p + \frac{2}{\pi} \int_0^\infty A(\alpha)\, e^{-\alpha y} \cos(\alpha x)\, d\alpha, \quad y > 0 \tag{C3}$$

Below the ground interface we have $(\nabla^2 + k_4^2)E_z = 0$, with k_4 the wavenumber in the ground, and

$$E_z = i\omega\frac{2}{\pi}\int_0^\infty A(\alpha)\, e^{-iy\sqrt{k_4^2-\alpha^2}}\cos(\alpha x)\, d\alpha, \quad y < 0 \tag{C4}$$

Matching E_z and H_x across the ground interface gives

$$A(\alpha) = \frac{-\frac{1}{2}\mu_0 I e^{-\alpha h}}{\alpha - i\frac{\mu_0}{\mu_4}\sqrt{k_4^2-\alpha^2}} \tag{C5}$$

The magnetic flux between the wire surface and infinity is $\Phi = -A_z(x = a, y = h)$, where the impedance per unit length is

$$Z = \frac{-i\omega\Phi}{I} = -i\omega\frac{\mu_0}{2\pi}\ln\left(\frac{2h}{a}\right) + Z^{fi} \tag{C6}$$

with the ground contribution as

$$Z^{fi} = -i\omega\frac{\mu_0}{\pi}\int_0^\infty \frac{1}{\alpha - i\frac{\mu_0}{\mu_4}\sqrt{k_4^2-\alpha^2}} e^{-2\alpha h} d\alpha \tag{C7}$$

The Hankel function approximation and the logarithm approximation to the single wire ground impedance are given by

$$\begin{aligned} Z^{fi} &= \frac{-i\omega\mu_0 H_0^{(1)}(k_4 h)}{2\pi k_4 h H_1^{(1)}(k_4 h)} \text{ Hankel} \\ Z^{fi} &= -i\omega\frac{\mu_0}{2\pi}\ln\left(\frac{1-ik_4 h}{-ik_4 h}\right) \text{ Logarithm} \end{aligned} \tag{C8}$$

A comparison of the ground impedance evaluated using the integral in Eq. (C7) with the two approximations in Eq. (C8) is reported in Fig. C1 versus frequency, showing that the three formulas provide with the same level of accuracy (see also [24]).

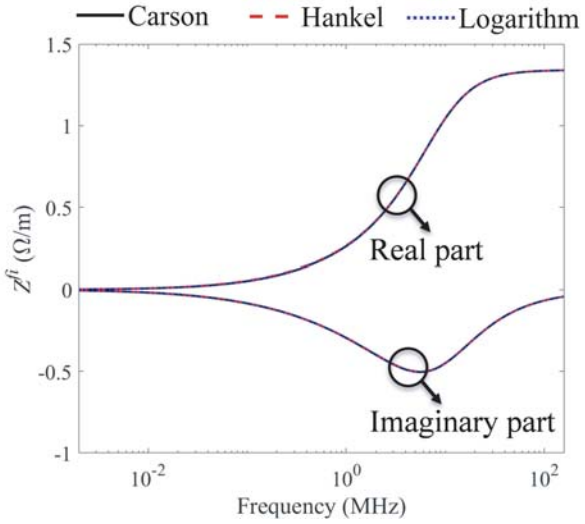

Figure C1. Ground impedance Z^{fi} versus frequency using Carson's integral, the approximation using the Hankel function, and the approximation using the logarithm function.

If there is an internal impedance Z_i associated with the wire because of wire conductivity σ_0, the contribution when the axial contour is taken inside the wire shows up in Faraday's law as

$$\oint_C E \cdot \underline{dl} = \frac{dV}{dz} = i\omega \left(\Phi + \Phi_i\right) = i\omega\Phi_{tot} = -Z_{tot} I \tag{C9}$$

with total impedance $Z_{tot} = Z + Z_i$.

Similarly, the voltage at the wire is $V = -\phi(x = a, y = h)$, with

$$\phi = \frac{q}{2\pi\varepsilon_0} \ln\left(\frac{\sqrt{x^2 + (y-h)^2}}{\sqrt{x^2 + (y+h)^2}}\right) \tag{C10}$$

leading to $C_e = q/V = 2\pi\varepsilon_0/\text{arcosh}(h/a) \approx 2\pi\varepsilon_0/\ln(2h/a)$, and $Y_e = -i\omega C_e$. If there is a ground admittance, the total admittance per unit length is $\frac{1}{Y} = \frac{1}{Y_e} + \frac{1}{Y^{fi}}$.

Sunde [3] suggested a semi-circular approximation to the ground admittance for lower frequencies [10, 11] but we neglect it in this paper for aerial lines.

The propagation constant for the mode supported by the single wire is $\Gamma = \sqrt{-ZY}$.

C.2. Common and Differential Modes of a Two-Wire System

For two wires carrying z-directed currents $-I_\pm$, we take

$$\begin{aligned} A_z^p &= \frac{\mu_0 I_+}{2\pi} \ln\left[\frac{\sqrt{(x-x_+)^2 + (y-h_+)^2}}{\sqrt{(x-x_+)^2 + (y+h_+)^2}}\right] + \frac{\mu_0 I_-}{2\pi} \ln\left[\frac{\sqrt{(x-x_-)^2 + (y-h_-)^2}}{\sqrt{(x-x_-)^2 + (y+h_-)^2}}\right] \\ &= -\frac{\mu_0 I_+}{2\pi} \int_0^\infty \left[e^{-\alpha|y-h_+|} - e^{-\alpha|y+h_+|}\right] \cos\left[\alpha\left(x - x_+\right)\right] \frac{d\alpha}{\alpha} \\ &\quad -\frac{\mu_0 I_-}{2\pi} \int_0^\infty \left[e^{-\alpha|y-h_-|} - e^{-\alpha|y+h_-|}\right] \cos\left[\alpha\left(x - x_-\right)\right] \frac{d\alpha}{\alpha} \end{aligned} \tag{C11}$$

with

$$\begin{aligned} A_z &= A_z^p + \frac{2}{\pi} \int_0^\infty \left\{A_+\left(\alpha\right) \cos\left[\alpha\left(x - x_+\right)\right] + A_-\left(\alpha\right) \cos\left[\alpha\left(x - x_-\right)\right]\right\} e^{-\alpha y} d\alpha, \quad y > 0 \\ E_z &= i\omega \frac{2}{\pi} \int_0^\infty \left\{A_+\left(\alpha\right) \cos\left[\alpha\left(x - x_+\right)\right] + A_-\left(\alpha\right) \cos\left[\alpha\left(x - x_-\right)\right]\right\} e^{-iy\sqrt{k_4^2 - \alpha^2}} d\alpha, \quad y < 0 \end{aligned} \tag{C12}$$

and

$$A_\pm\left(\alpha\right) = \frac{-\frac{1}{2}\mu_0 I_\pm e^{-\alpha h_\pm}}{\alpha - i\frac{\mu_0}{\mu_4}\sqrt{k_4^2 - \alpha^2}} \tag{C13}$$

The magnetic fluxes from a particular wire to the reference at infinity are $\Phi_{++} = -[A_z(x = x_+ + a_+, y = h_+)]_{I_-=0}$, $\Phi_{+-} = -[A_z(x = x_+ + a_+, y = h_+)]_{I_+=0}$, $\Phi_{-+} = -[A_z(x = x_- + a_-, y = h_-)]_{I_-=0}$, and $\Phi_{--} = -[A_z(x = x_- + a_-, y = h_-)]_{I_+=0}$, giving the following impedances

$$\begin{aligned} Z_{\pm\pm} &= \frac{-i\omega\Phi_{\pm\pm}}{I_\pm} = -i\omega\frac{\mu_0}{2\pi} \ln\left(\frac{2h_\pm}{a_\pm}\right) + Z_{\pm\pm}^{fi}, \\ Z_{\pm\mp} &= \frac{-i\omega\Phi_{\pm\mp}}{I_\mp} = -i\omega\frac{\mu_0}{2\pi} \ln\left(\frac{\sqrt{(x_+ - x_-)^2 + (h_+ + h_-)^2}}{\sqrt{(x_+ - x_-)^2 + (h_+ - h_-)^2}}\right) + Z_{\pm\mp}^{fi} \end{aligned} \tag{C14}$$

with the ground contributions

$$\begin{aligned} Z_{\pm\pm}^{fi} &= -i\omega\frac{\mu_0}{\pi}\int_0^\infty \frac{1}{\alpha - i\frac{\mu_0}{\mu_4}\sqrt{k_4^2-\alpha^2}}e^{-2\alpha h_+}d\alpha = Z^{fi}\left(h_\pm\right), \\ Z_{\pm\mp}^{fi} &= -i\omega\frac{\mu_0}{\pi}\int_0^\infty \frac{\cos\left[\alpha\left(x_+ - x_-\right)\right]}{\alpha - i\frac{\mu_0}{\mu_4}\sqrt{k_4^2-\alpha^2}}e^{-\alpha(h_+ + h_-)}d\alpha \\ &= \frac{1}{2}\left[Z^{fi}\left(\frac{(h_+ + h_-)}{2} + \frac{i\left(x_+ - x_-\right)}{2}\right) + Z^{fi}\left(\frac{(h_+ + h_-)}{2} - \frac{i\left(x_+ - x_-\right)}{2}\right)\right]. \end{aligned} \tag{C15}$$

It is clear that the two-wire ground impedance is obtained from the single-wire one in Eq. (C7), and so the two Hankel and logarithm approximations in Eq. (C8) can also be used here with the proper arguments as shown in Eq. (C14).

If there is an internal impedance Z_i associated with the wire because of wire conductivity, this is taken into account similar to Eq. (C9). This means that $Z_{\pm\pm} \to Z_{\pm\pm} + Z_{i\pm}$ but there is no change in the mutual terms since this internal flux is not captured (or in the other equivalent view there is no surface contour for the mutual terms on a conductor carrying current).

Similarly, the voltages at the wires are $V_{++} = -[\phi(x = x_+ + a_+, y = h_+)]_{q_-=0}$, $V_{+-} = -[\phi(x = x_+ + a_+, y = h_+)]_{q_+=0}$, $V_{-+} = -[\phi(x = x_- + a_-, y = h_-)]_{q_-=0}$, and $V_{--} = -[\phi(x = x_- + a_-, y = h_-)]_{q_+=0}$, with

$$\phi = \frac{q_+}{2\pi\varepsilon_0}\ln\left(\frac{\sqrt{(x-x_+)^2+(y-h_+)^2}}{\sqrt{(x-x_+)^2+(y+h_+)^2}}\right) + \frac{q_-}{2\pi\varepsilon_0}\ln\left(\frac{\sqrt{(x-x_-)^2+(y-h_-)^2}}{\sqrt{(x-x_-)^2+(y+h_-)^2}}\right) \tag{C16}$$

The side conditions here are open circuit conditions and consequently these are useful for determining the elastance matrix in $V = S \cdot q$, where

$$S = \begin{pmatrix} S_{++} & S_{+-} \\ S_{-+} & S_{--} \end{pmatrix}; \quad q = \begin{pmatrix} q_+ \\ q_- \end{pmatrix} \tag{C17}$$

and

$$S_{\pm\pm} = \frac{V_{\pm\pm}}{q_\pm} = \frac{1}{2\pi\varepsilon_0}\ln\left(\frac{2h_\pm}{a_\pm}\right), \quad S_{\pm\mp} = \frac{V_{\pm\mp}}{q_\mp} = \frac{1}{2\pi\varepsilon_0}\ln\left(\frac{\sqrt{(x_+-x_-)^2+(h_++h_-)^2}}{\sqrt{(x_+-x_-)^2+(h_+-h_-)^2}}\right) \tag{C18}$$

where we are approximating the elastances by the external contribution. The capacitance matrix is the inverse of the elastance matrix

$$C = \begin{pmatrix} C_{++} & C_{+-} \\ C_{-+} & C_{--} \end{pmatrix} = S^{-1} = \frac{1}{S_{++}S_{--} - S_{+-}S_{-+}}\begin{pmatrix} S_{++} & S_{+-} \\ S_{-+} & S_{--} \end{pmatrix} \tag{C19}$$

and the admittance matrix terms are given by $Y_{\pm\pm} = -i\omega C_{\pm\pm}$ and $Y_{\pm\mp} = -i\omega C_{\pm\mp}$.

C.3. Equivalent Radius Model for the Common Mode of a Two-Wire System

The local vector potential for two wires carrying $-z$-directed currents $I_\pm$ can be written as

$$A_z = \frac{\mu_0}{2\pi}\left\{I_+\ln\left[\sqrt{(x-x_+)^2+(y-h_+)^2}\right] + I_-\ln\left[\sqrt{(x-x_-)^2+(y-h_-)^2}\right]\right\} \tag{C20}$$

On each of the wires the potential is

$$A_z\left(x = x_\pm + a_\pm, y = h_\pm\right) = \frac{\mu_0}{2\pi}I_\mp\ln\left(2\Delta/a_\mp\right) \tag{C21}$$

where the distance between them is $2\Delta = \sqrt{(x_+-x_-)^2+(h_+-h_-)^2}$. Thus, to make the potential difference between the wires vanish (no magnetic flux between them) we impose $I_-\ln(2\Delta/a_-) =$

$I_+ \ln(2\Delta/a_+)$. Defining $I_+ + I_- = I$ and $I_+ - I_- = I_d$, leading to $I_+ = (I + I_d)/2$ and $I_- = (I - I_d)/2$, and writing the flux condition as $(I_+ - I_-)\ln(2\Delta) = I_+ \ln a_+ - I_- \ln a_-$, or $I_d \ln(2\Delta) = \frac{1}{2}(I + I_d)\ln a_+ - \frac{1}{2}(I - I_d)\ln a_-$, we can solve this as $\frac{I_d}{I} = \frac{\ln\sqrt{a_+/a_-}}{\ln(2\Delta) - \ln\sqrt{a_+ a_-}}$ and

$$I_\pm = \frac{1}{2}(I \pm I_d) = I\frac{\ln\sqrt{2\Delta/a_\mp}}{\ln(2\Delta) - \ln\sqrt{a_+ a_-}} \tag{C22}$$

Then the value on the wires is

$$A_z(x = x_\pm + a_\pm, y = h_\pm) = \frac{\mu_0}{\pi} I \frac{\ln\sqrt{2\Delta/a_+}\ln\sqrt{2\Delta/a_-}}{\ln(2\Delta) - \ln\sqrt{a_+ a_-}} \tag{C23}$$

At a large distance from the wires $\rho = \sqrt{x^2 + y^2} \gg 2\Delta, a_\pm$, the potential is $A_z \sim \frac{\mu_0}{2\pi}[I\ln\rho - I_+\ln a_+ - I_-\ln a_-]$. Subtracting the wire potential gives

$$A_z - A_z(x = x_\pm + a_\pm, y = h_\pm) \sim \frac{\mu_0}{2\pi}[I\ln\rho - I_+\ln a_+ - I_-\ln a_- - I_\mp \ln(2\Delta/a_\mp)] \tag{C24}$$

Now defining the equivalent radius a_e by $I\ln a_e = I_+\ln a_+ + I_-\ln a_- + I_\mp\ln(2\Delta/a_\mp)$ so that $A_z \sim \frac{\mu_0}{2\pi}\ln(\rho/a_e)$ with

$$\ln a_e = \frac{\ln\sqrt{2\Delta/a_-}\ln a_+ + \ln\sqrt{2\Delta/a_+}\ln a_- + 2\ln\sqrt{2\Delta/a_+}\ln\sqrt{2\Delta/a_-}}{\ln(2\Delta) - \ln\sqrt{a_+ a_-}} \tag{C25}$$

The result of this model is reported in Fig. C2 compared to the common mode result from the two-wire model in Fig. 6. We observe that for small separation $2\Delta \leq 5\,\mathrm{m} \ll h$ there is good agreement between the two formulations, as one would expect. However, the larger the separation $2\Delta \sim h$, the more the disagreement, as attested by the result for $2\Delta = 10\,\mathrm{m}$.

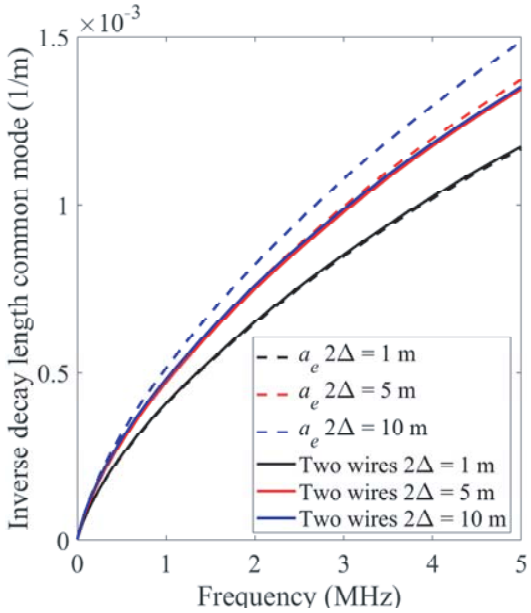

Figure C2. Inverse decay lengths for various values of separation 2Δ for the common mode using the equivalent radius formulation for two wires above ground with $h = 10\,\mathrm{m}$.

C.4. Line Quadrupole Moment Mode of a Three-wire System

We now consider three wires carrying z-directed currents $I_0 = -I$ and $I_\pm = I/2$ at heights $h_\pm = h$ and $h_0 = h$ with horizontal separation $x_\pm = x_0$. We thus take

$$\begin{aligned} A_z^p &= \frac{\mu_0 I}{2\pi}\ln\left[\frac{\sqrt{x^2+(y-h)^2}}{\sqrt{x^2+(y+h)^2}}\right] - \frac{\mu_0 I}{4\pi}\ln\left[\frac{\sqrt{(x-x_0)^2+(y-h)^2}}{\sqrt{(x-x_0)^2+(y+h)^2}}\right] - \frac{\mu_0 I}{4\pi}\ln\left[\frac{\sqrt{(x+x_0)^2+(y-h)^2}}{\sqrt{(x+x_0)^2+(y+h)^2}}\right] \\ &= -\frac{\mu_0 I}{2\pi}\int_0^\infty \left[e^{-\alpha|y-h|} - e^{-\alpha|y+h|}\right]\cos[\alpha x]\frac{d\alpha}{\alpha} + \frac{\mu_0 I}{4\pi}\int_0^\infty \left[e^{-\alpha|y-h|} - e^{-\alpha|y+h|}\right]\cos[\alpha(x-x_0)]\frac{d\alpha}{\alpha} \\ &\quad + \frac{\mu_0 I}{4\pi}\int_0^\infty \left[e^{-\alpha|y-h|} - e^{-\alpha|y+h|}\right]\cos[\alpha(x+x_0)]\frac{d\alpha}{\alpha} \\ &= -\frac{\mu_0 I}{2\pi}\int_0^\infty \left[e^{-\alpha|y-h|} - e^{-\alpha|y+h|}\right][1-\cos[\alpha x]]\frac{d\alpha}{\alpha} \end{aligned} \tag{C26}$$

with

$$\begin{aligned} A_z &= A_z^p + \frac{2}{\pi}\int_0^\infty A_0(\alpha)[1-\cos[\alpha x_0]]e^{-\alpha y}\cos(\alpha x)\,d\alpha, \quad y>0 \\ E_z &= i\omega\frac{2}{\pi}\int_0^\infty A_0(\alpha)[1-\cos[\alpha x_0]]e^{-iy\sqrt{k_4^2-\alpha^2}}\cos(\alpha x)\,d\alpha, \quad y<0 \end{aligned} \tag{C27}$$

and

$$A_0(\alpha) = \frac{-\frac{1}{2}\mu_0 I e^{-\alpha h}}{\alpha - i\frac{\mu_0}{\mu_4}\sqrt{k_4^2-\alpha^2}} \tag{C28}$$

The impedance is equal to

$$Z = -i\omega\frac{\mu_0}{\pi}\ln\sqrt{\frac{2hx_0^2\sqrt{2h\sqrt{x_0^2+h^2}}}{a_0\sqrt{a|x_0|}\left[x_0^2+(2h)^2\right]}} + Z_{3w}^{fi} + \frac{3}{2}Z_i \tag{C29}$$

with ground impedance

$$\begin{aligned} Z_{3w}^{fi} &= -i\omega\frac{\mu_0}{\pi}\int_0^\infty \frac{[1-\cos(\alpha x)]^2}{\alpha - i\frac{\mu_0}{\mu_4}\sqrt{k_4^2-\alpha^2}}e^{-2\alpha h}d\alpha \\ &= \frac{3}{2}Z^{fi}(h) - Z^{fi}\left(h+i\frac{x_0}{2}\right) - Z^{fi}\left(h-i\frac{x_0}{2}\right) + \frac{1}{4}Z^{fi}(h-ix_0) + \frac{1}{4}Z^{fi}(h+ix_0), \end{aligned} \tag{C30}$$

and the admittance is $Y = Y_e$ with

$$Y_e = \frac{-i\omega\pi\varepsilon_0}{\ln\sqrt{\frac{2hx_0^2\sqrt{2h\sqrt{x_0^2+h^2}}}{a_0\sqrt{a|x_0|}\left[x_0^2+(2h)^2\right]}}} \tag{C31}$$

These immittances in Eqs. (C29), (C30), and (C31) were evaluated using a complex power definition for the composite differential mode. The potential for the three line sources $I_0 = -I$ and $I_\pm = I/2$ of the composite differential mode satisfies the equation

$$\nabla_t^2 A_z = -\mu_0 J_z = \mu_0 I\delta(x)\delta(y-h) - \mu_0\frac{I}{2}\delta(x-x_0)\delta(y-h) - \mu_0\frac{I}{2}\delta(x+x_0)\delta(y-h) \tag{C32}$$

where $\nabla_t = \underline{e}_x \delta/\delta x + \underline{e}_y \delta/\delta y$ is the transverse Laplacian operator. Taking the conjugate, multiplying by A_z and using the identity

$$\begin{aligned} &\nabla_t \cdot (A_z \nabla_t A_z^*) - \nabla_t A_z \cdot \nabla_t A_z^* \\ &= A_z \nabla_t^2 A_z^* = \left[\mu_0 I^* \delta(x)\,\delta(y-h) - \mu_0 \frac{I^*}{2}\delta(x-x_0)\,\delta(y-h) - \mu_0 \frac{I^*}{2}\delta(x+x_0)\,\delta(y-h)\right] A_z \end{aligned} \quad \text{(C33)}$$

Integrating over the volume and using the divergence theorem gives

$$\oint_S A_z (\underline{e}_z \times \underline{B}_t^*) \cdot \underline{n} dS - \int_V \underline{B}_t \cdot \underline{B}_t^* dV = \mu_0 I^* A_z(a_0, h)\,\ell - \mu_0 \frac{I^*}{2}\left[A_z(a+x_0,h) + A_z(a-x_0,h)\right]\ell \quad \text{(C34)}$$

where we have used $\underline{B}_t = \mu_0 \underline{H}_t = \nabla \times \underline{A} = \nabla_t \times (A_z \underline{e}_z) = -\underline{e}_z \times \nabla_t A_z$ and we have taken the volume to have a length ℓ in the z direction. We take the closed surface S to consist of a semi-circular surface (which we will take to infinity), two fixed surfaces in z (which vanish when $\underline{n} = \pm \underline{e}_z$), and the surface of the ground to be S_0. Dividing by μ_0 and multiplying by $i\omega$, where on the ground surface we take $E_z = i\omega A_z$

$$\begin{aligned} &\oint_{S_0} E_z (\underline{e}_z \times \underline{H}_t^*) \cdot \underline{n} dS - i\omega \int_V \mu_0 \underline{H}_t \cdot \underline{H}_t^* dV \\ &= i\omega I^* A_z(a_0, h)\,\ell - i\omega \frac{I^*}{2}\left[A_z(a+x_0,h) + A_z(a-x_0,h)\right]\ell \end{aligned} \quad \text{(C35)}$$

Noting that $E_z \underline{n} \cdot (\underline{e}_z \times \underline{H}_t^*) = \underline{n} \cdot (E_z \underline{e}_z \times \underline{H}_t^*) = 2\underline{n} \cdot \underline{S}$ where here we are denoting the complex Poynting vector by $\underline{S} = \underline{E} \times \underline{H}^*/2$, we see from the Poynting theorem that twice the complex power radiated by the current is

$$\begin{aligned} 2P &= \oint_{S_0} E_z (\underline{e}_z \times \underline{H}_t^*) \cdot \underline{n} dS - i\omega \int_V \mu_0 \underline{H}_t \cdot \underline{H}_t^* dV \\ &= i\omega I^* A_z(a_0, h)\,\ell - i\omega \frac{I^*}{2}\left[A_z(a+x_0,h) + A_z(a-x_0,h)\right]\ell \end{aligned} \quad \text{(C36)}$$

Setting this equal to the voltage per unit length along the line $-E_z$ times the conjugate of the current (noting that the current is oppositely directed to $\underline{e}_z$ so that $E_z = -ZI$) times the length ℓ gives

$$2P = -E_z I^* \ell = Z I I^* \ell \quad \text{(C37)}$$

or

$$\begin{aligned} ZI &= i\omega A_z(a_0, h) - i\omega \frac{1}{2}\left[A_z(a+x_0,h) + A_z(a-x_0,h)\right] \\ &= \frac{-i\omega\mu_0 I}{\pi} \ln \sqrt{\frac{2h x_0^2 \sqrt{2h\sqrt{x_0^2+h^2}}}{a_0 \sqrt{a\,|x_0|}\left[x_0^2 + (2h)^2\right]}} + Z_{3w}^{fi} I \end{aligned} \quad \text{(C38)}$$

Similarly for the transverse electric field problem we take the charges per unit length $q_0 = -q$ and $q_\pm = q/2$ and the scalar potential satisfies

$$\nabla_t^2 \phi = \frac{q}{\varepsilon_0}\delta(x)\,\delta(y-h) - \frac{q}{2\varepsilon_0}\delta(y-h)\left[\delta(x-x_0) + \delta(x+x_0)\right] \quad \text{(C39)}$$

The identity $\nabla_t \cdot (\phi \nabla_t \phi^*) - \nabla_t \phi \cdot \nabla_t \phi^* = \phi \nabla_t^2 \phi^*$ and relation $\underline{E}_t = -\nabla_t \phi = \underline{D}_t/\varepsilon_0$ when integrated over the volume gives

$$\oint_S \phi \underline{D}_t^* \cdot \underline{n} dS - \int_V \varepsilon_0 \underline{E}_t \cdot \underline{E}_t^* dV = q^* \phi(a_0, h)\,\ell - \frac{q^*}{2}\left[\phi(a+x_0,h) + \phi(a-x_0,h)\right]\ell \quad \text{(C40)}$$

Then by the same argument $\oint\limits_S \phi \underline{D}_t^* \cdot \underline{n} dS \to \oint\limits_{S_0} \phi \underline{D}_t^* \cdot \underline{n} dS$, for the external admittance we take $\phi = 0$ on S_0 to find

$$\int\limits_V \varepsilon_0 \underline{E}_t \cdot \underline{E}_t^* dV = -q^* \phi(a_0, h) + \frac{q^*}{2} \left[\phi(a + x_0, h) + \phi(a - x_0, h)\right]$$

$$= S_e q q^* = q q^* / C_e = \frac{q q^*}{\pi \varepsilon_0} \ln \sqrt{\frac{2h x_0^2 \sqrt{2h\sqrt{x_0^2 + h^2}}}{a_0 \sqrt{a |x_0|} \left[x_0^2 + (2h)^2\right]}} \tag{C41}$$

REFERENCES

1. Xie, H., T. Du, M. Zhang, Y. Li, H. Qiao, J. Yang, et al., "Theoretical and experimental study of effective coupling length for transmission lines illuminated by HEMP," *IEEE Transactions on Electromagnetic Compatibility*, Vol. 57, 1529–1538, 2015.
2. Carson, J. R., "Wave propagation in overhead wires with ground return," *The Bell System Technical Journal*, Vol. 5, 539–554, 1926.
3. Sunde, E. D., *Earth Conduction Effects in Transmission Systems*, Dover, New York, 1967.
4. Wait, J. R., "Theory of wave propagation along a thin wire parallel to an interface," *Radio Science*, Vol. 7, 675–679, 1972.
5. Wait, J. R., "Tutorial note on the general transmission line theory for a thin wire above the ground," *IEEE Transactions on Electromagnetic Compatibility*, Vol. 33, 65–67, 1991.
6. Chang, D. and J. Wait, "Extremely Low Frequency (ELF) propagation along a horizontal wire located above or buried in the Earth," *IEEE Transactions on Communications*, Vol. 22, 421–427, 1974.
7. Kuester, E. F., D. C. Chang, and S. W. Plate, "Electromagnetic wave propagation along horizontal wire systems in or near a layered Earth," *Electromagnetics*, Vol. 1, 243–265, January 1, 1981.
8. Olsen, R. G., J. L. Young, and D. C. Chang, "Electromagnetic wave propagation on a thin wire above Earth," *IEEE Transactions on Antennas and Propagation*, Vol. 48, 1413–1419, 2000.
9. Kuester, E. F., D. C. Chang, and R. G. Olsen, "Modal theory of long horizontal wire structures above the Earth: 1, Excitation," *Radio Science*, Vol. 13, 605–613, 1978.
10. Campione, S., L. K. Warne, L. I. Basilio, C. D. Turner, K. L. Cartwright, and K. C. Chen, "Electromagnetic pulse excitation of finite- and infinitely-long lossy conductors over a lossy ground plane," *Journal of Electromagnetic Waves and Applications*, Vol. 31, 209–224, 2017.
11. Warne, L. K. and K. C. Chen, "Long line coupling models," *Sandia National Laboratories Report*, Vol. SAND2004-0872, Albuquerque, NM, 2004.
12. Vance, E. F., *Coupling to Shielded Cables*, R. E. Krieger, 1987.
13. Lee, K. S. H., *EMP Interaction: Principles, Techniques, and Reference Data*, Hemisphere Publishing Corp., Washington, 1986.
14. Tesche, F. M., M. V. Ianoz, and T. Karlsson, *EMC Analysis Methods and Computational Models*, John Wiley & Sons, Inc., New York, 1997.
15. Olsen, R. G. and A. G. Tarditi, "EMP coupling to a straight conductor above ground: Transmission line formulation based on electromagnetic reciprocity," *IEEE Transactions on Electromagnetic Compatibility*, 1–9, 2018.
16. Ianoz, M., B. I. C. Nicoara, and W. A. Radasky, "Modeling of an EMP conducted environment," *IEEE Transactions on Electromagnetic Compatibility*, Vol. 38, 400–413, 1996.
17. Campione, S., L. K. Warne, R. L. Schiek, and L. I. Basilio, "Electromagnetic pulse excitation of finite-long dissipative conductors over a conducting ground plane in the frequency domain," *Sandia National Laboratories Report*, Vol. SAND2017-10078, Albuquerque, NM, 2017.

18. Warne, L. K. and S. Campione, "Formulas for plane wave coupling to a transmission line above ground with terminating loads," *Sandia National Laboratories Report*, Vol. SAND2018-8736, Albuquerque, NM, 2018.
19. Baum, C. F., "Effect of corona on the response of infinite-length transmission lines to incident plane waves," *AFWL Interaction Note*, Vol. 443, February 6, 1985.
20. Blanchard, J. P., "A calculational model of corona effects on conducting wire in a High Altitude Electromagnetic Pulse (HEMP) environment," *AFWL Interaction Note*, Vol. 455, November 21, 1985.
21. Lee, K. S. H., "Electromagnetic coupling to transmission lines," *Electromagnetics*, Vol. 8, 107–124, January 1, 1988.
22. Hoad, R. and W. A. Radasky, "Progress in High-Altitude Electromagnetic Pulse (HEMP) standardization," *IEEE Transactions on Electromagnetic Compatibility*, Vol. 55, 532–538, 2013.
23. *EMP Engineering and Design Principles*, Whippany, NJ, 1975.
24. Chen, K. C. and K. M. Damrau, "Accuracy of approximate transmission line formulas for overhead wires," *IEEE Transactions on Electromagnetic Compatibility*, Vol. 31, 396–397, 1989.